The phase diagram of the two center Lennard-Jones model as obtained from computer simulation and Wertheim's thermodynamic perturbation theory

C. Vega[a] and C. McBride
Departamento de Química Física, Facultad de Ciencias Químicas, Universidad Complutense de Madrid, Ciudad Universitaria 28040 Madrid, Spain

E. de Miguel and F. J. Blas
Departamento de Física Aplicada, Facultad de Ciencias Experimentales, Universidad de Huelva, 21071, Huelva, Spain

A. Galindo
Department of Chemical Engineering and Chemical Technology, Imperial College, London, South Kensington Campus, London SW7 2AZ United Kingdom

(Received 24 January 2003; accepted 14 March 2003)

The global phase diagram (i.e., vapor–liquid and fluid–solid equilibrium) of two-center Lennard-Jones (2CLJ) model molecules of bond length $L=\sigma$ has been determined by computer simulation. The vapor–liquid equilibrium conditions are obtained using the Gibbs ensemble Monte Carlo method and by performing isobaric-isothermal NPT calculations at zero pressure. In the case of the solid phase, two close-packed solid structures are considered: In the first structure, the molecules are located in layers and all molecular axes point in the same direction; and in the second structure, the atoms form a close-packed arrangement but the molecular axes of the diatomic molecules have random orientations. It is shown that at the vapor–liquid–solid triple-point temperature, the orientationally disordered solid is the stable structure for the solid phase of this model. The vapor–liquid-disordered solid triple-point temperature of the 2CLJ model, with bond length $L=\sigma$, is located at $T^*=0.650(4)$. This is very close to the triple-point temperature of the Lennard-Jones monomer system ($T^*=0.687$). At very low temperatures, the ordered solid is the stable phase. The vapor-ordered solid-disordered solid triple point is situated at $T^*=0.282$. The simulation data are compared to Wertheim's first-order thermodynamic perturbation theory (TPT1) for the fluid and solid phases. It is found that Wertheim's TPT1 not only provides an accurate description of the equation of state in both the fluid and solid phases, but also provides accurate values of the free energies. The prediction of Wertheim's TPT1 for the global phase diagram of the 2CLJ model shows excellent agreement with the simulation results, illustrating the possibility of using Wertheim's perturbation theory to determine not only the vapor–liquid equilibria but also the global phase diagram of simple chain model molecules. © *2003 American Institute of Physics*. [DOI: 10.1063/1.1572811]

I. INTRODUCTION

Since the initial computer simulations in the 1950's, a considerable amount of work has been devoted to the determination of the phase diagrams of model molecular systems. The calculation, by means of computer simulation, of the phase diagrams of the hard-sphere[1,2] and Lennard-Jones monomer systems[3] have played an important role in improving our understanding of the states of matter. In the last twenty years, the phase diagrams of a number of model systems (including solid and liquid-crystalline phases) have been obtained by using computer simulation. For example, studies have been carried out for hard ellipsoids,[4] hard spherocylinders,[5] hard cut spheres,[6] hard dumbbells,[7–9] quadrupolar hard dumbbells,[10] fully flexible hard chains,[11,12] hard charged spheres,[13–15] Gay–Berne molecules,[16,17] and simple point charge model water molecules.[18]

The calculation of the complete phase diagram of a proposed model system can now be carried out within a reasonable amount of time due to the increased speed of modern computers. However, brute force computational power is not the only key to the success of simulation studies; much credit is due to the development of simulation techniques for the determination of phase equilibria. These techniques are the Gibbs ensemble Monte Carlo[19] and the NPT+test particle methods,[20] which are very useful in determining the vapor–liquid equilibria, the Gibbs–Duhem integration method,[21,22] which becomes an invaluable tool when determining fluid–solid equilibria, the Rahman–Parrinello technique, essential in the study of solid phases,[23,24] and Einstein-crystal calculations, which provide the free energies of solid phases.[25] A general approach to the determination of global phase diagrams by computer simulation would entail:

[a]Electronic mail: cvega@eucmos.sim.ucm.es

(a) Obtaining the vapor–liquid equilibria using the Gibbs ensemble Monte Carlo technique (or the NPT+test particle method), and determining the orthobaric densities at low pressures by carrying out NPT simulations at zero pressure.
(b) Determining the equation of state (EOS) of the solid for one isotherm using the Rahman–Parrinello technique (or one of its Monte Carlo counterparts), and performing free-energy calculations in the equilibrium unit cell using Einstein-crystal calculations.
(c) Performing a Gibbs–Duhem integration to obtain the complete fluid–solid equilibrium curve.

These are the steps that have been followed in the determination of the global phase diagram of model two-center Lennard-Jones (2CLJ) molecules studied in this work.

Following the success of the Lennard-Jones (LJ) intermolecular potential as a model for atomic fluids, one of the simplest molecular models that can be proposed is the 2CLJ. This model consists of two LJ centers with potential parameters ϵ and σ separated from one another by a reduced bond length of $L^*=L/\sigma$. The vapor–liquid equilibria of 2CLJ model molecules with different values of L^* has been studied by a number of authors,[26–30] and has been the subject of interest in a large number of theoretical studies.[31–35] Somewhat surprisingly, the fluid–solid equilibria has not been considered in detail, the only exception being the work of Lisal and Vacek[36] who have determined the global phase diagram (vapor–liquid–solid) for a 2CLJ system with $L^*=0.67$ by molecular-dynamics computer simulations and using the Gibbs–Duhem integration method.

In terms of theoretical developments in the field of perturbation theory and equations of state of complex fluids, in the 1980's Wertheim[37–40] presented a series of seminal papers developing a theory for associating fluids. It has since been shown that when the association strength becomes infinitely strong, chains can be formed from a fluid of associating monomers,[41,42] thus, an EOS for a chain composed of freely jointed tangent monomers can be derived solely using the thermodynamic information of the monomer reference fluid. In the simplest implementation of the theory, known as first-order thermodynamic perturbation theory (TPT1), the only information required to build an approximate EOS for the chain fluid is the EOS and the pair correlation function of the monomer fluid at contact. Although Wertheim's formalism was originally aimed at the study of hard chains, it was soon realized that it could also be applied to LJ chains.[43–47]

Recently, we have explored the possibility of furthering the usefulness of Wertheim's TPT1 by applying it to the solid phase. Vega and MacDowell[48] have shown that Wertheim's TPT1 can be employed in the treatment of the solid phase for freely jointed hard-sphere chain molecules, obtaining excellent agreement with the simulation results of Malanoski and Monson.[11] This work has been extended by Blas *et al.*[49] to deal with fully flexible hard-chain molecules with segment–segment attractive interactions treated at the mean-field level of van der Waals. Similar results have also been obtained in two dimensions.[50] Encouraged by these findings, we have extended Wertheim's TPT1 to model the solid phase of LJ chains,[51] and have been able to show that the approach provides a good description of the EOS and good results for the internal energy of the solid phase of LJ tangent dimers (2CLJ with $L^*=1$). It is important to note that Wertheim's TPT1 can only be used to describe chains formed by ''tangent'' spheres (i.e., those with reduced bond lengths $L^*=1$). Since Wertheim's TPT1 can provide an accurate description of the EOS of the 2CLJ model with $L^*=1$ in the fluid and solid phases, it is natural to wonder whether it could be used to describe the global phase diagram of the 2CLJ model. It is important to mention at this stage that an accurate EOS for the solid phase does not necessarily guarantee the correct prediction of the fluid–solid equilibria, as the theoretical approach must also provide good estimates for the free energies in the solid phase. In this work, we determine the phase diagram of the 2CLJ model (with $L^*=1$) using computer simulations, and we compare the phase diagram obtained in this way with that obtained using Wertheim's TPT1.

The study of the solid phases of 2CLJ model molecules implies that a number of structures should be considered. While a system of LJ monomers freezes into a face-centered-cubic (fcc) close-packed arrangement, in the case of 2CLJ molecules with $L^*=1$, it is possible to construct, based on the closed-packed configuration of the LJ monomer solid, a number of distinct solid structures. Vega, Paras, and Monson[8] have presented several structures of this type for hard diatomic (hard dumbbell) molecules; each of the arrangements are possible configurations for 2CLJ molecules. In these structures, the molecules are located in layers, and the molecular axes of all the molecules in a layer point in the same direction. In the particular case of the so-called closed-packed 1 (CP1) structure, the molecular axes of each of the molecules in each of the layers point in the same direction. In the present work, the CP1 configuration is considered as one of the possible solid structures of the 2CLJ tangent model. This CP1 solid structure will be denoted as the ordered solid. It was found in Ref. 8 that the differences between the free energies of different ordered solid structures were small, indicating that the CP1 is a good representative of these ordered structures. However, it is unlikely that ordered structures correspond to the stable solid phase for the 2CLJ tangent model. Wojciechowski, and co-workers[52,53] were the first to suggest that for $L^*=1$, it is possible to build a solid structure where the atoms follow an fcc close-packed arrangement, but where the bonds are randomly located within the solid, with no long-range orientational order between the bond vectors. We also consider this structure in this work and denote it the disordered solid. In fact, Wojciechowski *et al.*[52,53] have shown that the stable solid structure of tangent hard-disk dimers in two dimensions is formed by a close-packed arrangement of atoms with a disordered arrangement of bonds. The same idea holds true for hard chains in three dimensions,[11] and one may expect that the same would occur for a three-dimensional 2CLJ tangent dimer. In this work, it will be shown that the disordered solid is the stable solid structure for most thermodynamic conditions (with the exception of very low temperatures).

This article is organized as follows: In Sec. II, the extension of Wertheim's theory to model solid phases of LJ chains

is described, in Sec. III, we provide details of the computer simulations performed in this work, in Sec. IV, the results are presented, and in Sec. V, conclusions are discussed.

II. BRIEF DESCRIPTION OF WERTHEIM'S PERTURBATION THEORY

It is now well known that Wertheim's TPT1 can be used to describe the properties of LJ chains in the fluid phase.[54] This was first suggested by Chapman,[43] and later confirmed by Johnson *et al.*[45] The possibility of extending Wertheim's TPT1 to treat solid phases has only recently been explored.[48,50,51] It has been shown that an accurate description of the EOS and internal energies of the 2CLJ tangent model in the solid phase can be obtained following the ideas of the TPT1 theory of Wertheim. Details of the extension of Wertheim's TPT1 to model solid phases of LJ chains have been given elsewhere;[51] here, we provide only an overview of the main features of the approach.

Let us assume that we have a certain number N^{ref} of spherical monomer particles within a volume V at temperature T. These spherical particles interact through a spherical pair potential $u^{\mathrm{ref}}(r)$; in this work, the pair potential $u^{\mathrm{ref}}(r)$ is the LJ potential with parameters σ and ϵ. We denote this fluid as the reference fluid, and label its properties with the superscript ref. Let us also assume that in another container of volume V at temperature T, we have $N=N^{\mathrm{ref}}/m$ fully flexible chains of m monomers each. By fully flexible chains, we mean chains of m monomers with fixed bond lengths between monomers $L=\sigma$, and no other constraints (i.e., there is no restriction of either the bonding angles or of the torsional angles). Each monomer of a given chain interacts with all the other monomers in the system, either in the same molecule, or in other molecules, with the only exception of the monomer/s to which it is bonded, interacting via the pair potential $u^{\mathrm{ref}}(r)$. The chain system described so far will be denoted as the chain fluid. It follows from Wertheim's TPT1 that the free energy A of the chain model system can be written as

$$\frac{A}{Nk_BT}=\ln(\rho\sigma^3)-1+m\frac{A^{\mathrm{ref}}_{\mathrm{residual}}}{N^{\mathrm{ref}}k_BT}-(m-1)\ln y^{\mathrm{ref}}(\sigma), \tag{1}$$

where k_B is Boltzmann's constant, and $\rho=N/V$ the molecular number density. In Eq. (1), we have set the de Broglie thermal wavelength to σ. This expression indicates that the free energy of the chain may be obtained from a knowledge of the residual free energy of the reference fluid $A^{\mathrm{ref}}_{\mathrm{residual}}$ and the background pair correlation function $y^{\mathrm{ref}}(\sigma)$ of the reference fluid at the bonding distance σ.[55,56] As $y(r)=\exp[u(r)/k_BT]g(r)$, and since in the case of the LJ potential model the pair potential is zero at $r=\sigma$, for this particular choice of bond length, $y(\sigma)=g(\sigma)$. Replacing $y(\sigma)$ by $g(\sigma)$ in Eq. (1), and differentiating the free energy with respect to density, the EOS is given by

$$Z=mZ^{\mathrm{ref}}-(m-1)\left(1+\rho^{\mathrm{ref}}\frac{\partial \ln g^{\mathrm{ref}}(\sigma)}{\partial\rho^{\mathrm{ref}}}\right), \tag{2}$$

where we have defined the compressibility factor of the reference monomer system as $Z^{\mathrm{ref}}=P^{\mathrm{ref}}/(\rho^{\mathrm{ref}}k_BT)$, with P being the pressure. The corresponding residual part of the internal energy U is given by

$$\frac{U}{Nk_BT}=m\frac{U^{\mathrm{ref}}}{N^{\mathrm{ref}}k_BT}+(m-1)T\left(\frac{\partial \ln g^{\mathrm{ref}}(\sigma)}{\partial T}\right). \tag{3}$$

We denote Eqs. (1)–(3) as Wertheim's TPT1 theory.

It is useful to note here that the arguments used to derive Eqs. (1)–(3) make no special mention of the actual nature of the phase considered,[48,57,58] thus, this approach can be used to describe both fluid and solid phases. In such a case, all that is needed in order to obtain a unified theory for the global phase equilibria of chain molecules is the residual free energy, compressibility factor, and pair correlation function of the monomer system both in the fluid and solid phases. Johnson *et al.*[44,45] have provided values of the free energy and structural properties [i.e., $g^{\mathrm{ref}}(\sigma)$] for the monomer LJ fluid. In this work, we follow their implementation of the TPT1 of Wertheim to model the fluid phases of 2CLJ molecules.

Van der Hoef[59] has recently presented an analytical expression for the free energy of the LJ monomer solid obtained by fitting the most recent simulation results for the solid phase of this model to a simple functional expression. We shall use his expression in this work. Values of $g^{\mathrm{ref}}(\sigma)$ for the LJ monomer solid, which are also required in the TPT1 approach, were obtained by computer simulation in a previous work[51] for a number of temperatures and densities. The simulations results for $g^{\mathrm{ref}}(\sigma)$ were fitted to an empirical expression of the same polynomial form than that proposed by Johnson *et al.*[45] for the fluid phase; the coefficients of the polynomial can be found in Ref. 51.

III. SIMULATION DETAILS

In this work, we consider diatomic LJ model molecules formed by two identical LJ sites (monomers) with a bond distance $L=\sigma$, where σ is the diameter of the LJ monomer (i.e., the monomers are tangential). We shall refer to the model molecules as 2CLJ tangent. The pair interaction between a pair of molecules is given by

$$u(1,2)=\sum_{i=1}^{i=2}\sum_{j=1}^{j=2}4\epsilon\left[\left(\frac{\sigma}{r_{ij}}\right)^{12}-\left(\frac{\sigma}{r_{ij}}\right)^{6}\right], \tag{4}$$

where r_{ij} is the distance between site (monomer) i of molecule 1 and site j of molecule 2. In order to determine the global phase diagram of the 2CLJ tangent molecules, we have used various simulation techniques. Before describing the details of each technique, it is useful to note that in all the simulations performed, the site–site LJ pair potential was truncated at $r_c=2.5\sigma$, and long-range corrections were added to all the computed thermodynamic properties (internal energy, pressure, and chemical potential) by assuming that the site–site pair correlation function is equal to unity beyond the cutoff.[60] A cycle is defined as a trial move per particle, and a trial volume change. In the case of the Gibbs ensemble simulations, a cycle also includes N_{ex} attempts to exchange particles between the boxes. Throughout this work,

TABLE I. Vapor–liquid coexistence properties for the 2CLJ model with $L^*=1$ as obtained from Gibbs ensemble Monte Carlo simulations for systems containing initially 500+500 molecules. ρ^* indicates the reduced number density of molecules $\rho^*=N/V\sigma^3$, U^* is the residual internal energy per particle in units of ϵ, the pressure P^* is in units of ϵ/σ^3, and the chemical potential μ^* is in units of ϵ. The reported pressures and chemical potentials refer to values in the vapor phase (these values are equal to the corresponding values in the liquid phase within the statistical uncertainties).

T^*	ρ_v^*	ρ_ℓ^*	U_v^*	U_ℓ^*	P^*	μ^*
1.76	0.0822(58)	0.2116(158)	−2.260(151)	−5.07(32)	0.0723(19)	−6.30(2)
1.75	0.0729(46)	0.2180(147)	−2.034(124)	−5.22(31)	0.0686(18)	−6.32(3)
1.74	0.0677(61)	0.2225(116)	−1.902(171)	−5.33(24)	0.0655(24)	−6.33(3)
1.72	0.0645(43)	0.2412(56)	−1.840(110)	−5.75(12)	0.0625(20)	−6.31(2)
1.70	0.0543(31)	0.2472(63)	−1.583(87)	−5.89(14)	0.0564(19)	−6.34(2)
1.65	0.0421(28)	0.2658(50)	−1.276(85)	−6.35(12)	0.0463(17)	−6.37(3)
1.60	0.0322(22)	0.2812(34)	−1.010(68)	−6.75(8)	0.0372(17)	−6.42(4)
1.55	0.0262(14)	0.2972(28)	−0.849(49)	−7.17(7)	0.0305(12)	−6.44(3)
1.50	0.0205(12)	0.3097(19)	−0.689(38)	−7.51(5)	0.0243(10)	−6.49(4)
1.45	0.0158(10)	0.3224(25)	−0.549(37)	−7.87(6)	0.0189(10)	−6.54(5)
1.40	0.011 97(54)	0.3334(20)	−0.431(22)	−8.19(5)	0.014 33(55)	−6.61(4)
1.35	0.009 46(35)	0.3440(21)	−0.355(15)	−8.51(6)	0.011 18(35)	−6.63(3)
1.30	0.006 78(45)	0.3539(17)	−0.263(19)	−8.81(5)	0.007 96(47)	−6.74(6)
1.20	0.003 53(14)	0.3725(18)	−0.149(7)	−9.39(5)	0.003 98(15)	−6.92(4)
1.10	0.001 55(5)	0.3898(16)	−0.073(3)	−9.96(5)	0.001 65(5)	−7.19(3)
1.00	0.000 60(3)	0.4061(12)	−0.032(2)	−10.50(4)	0.000 59(3)	−7.45(4)

we use reduced units, so that $T^*=T/(\epsilon/k_B)$, $\rho^*=\rho\sigma^3=(N/V)\sigma^3$, $P^*=P/(\epsilon/\sigma^3)$, and $U^*=U/(N\epsilon)$.

A. Vapor–liquid equilibria

The vapor–liquid equilibria of the 2CLJ model has already been considered by a number of authors. Using Gibbs ensemble simulations, Dubey *et al.*[26] have obtained the vapor–liquid equilibria of the 2CLJ model system for several bond lengths, including $L^*=1$. More recently, Stoll *et al.*[28] have studied the vapor–liquid transitions for this model using the NPT+test particle method. In the latter work, special emphasis was placed on the accurate determination of the critical properties of the system; however, in order to compare this with our theoretical calculations, which incorporate the description of the solid phase as well as the fluid phases, we also have an interest in locating the triple point of the 2CLJ model. In this way, computer simulation data of the vapor–liquid equilibria at lower temperatures than reported previously is needed.

We have obtained the vapor–liquid properties of the 2CLJ model fluid with $L^*=1$ using the standard Gibbs ensemble Monte Carlo simulation technique. At each temperature T^*, an initial configuration is generated by first equilibrating two subsystems (each containing 500 molecules) at the given T^*, and with initial vapor and liquid densities close to the expected coexistence values. Constant-volume NVT Monte Carlo simulations are carried out in this equilibration stage, which consisted of approximately 10 000–20 000 cycles. The resulting configurations are subsequently used as starting configurations for the Gibbs ensemble run, which consisted of 50 000 equilibration cycles and 50 000 cycles for collecting averages. The coexistence densities, internal energies, pressures, and chemical potentials for each of the temperatures considered are presented in Table I.

At low temperatures, the probability of transferring particles between the two subsystems becomes extremely low (of the order of 1.9×10^{-5} at $T^*=1.0$) and, therefore, the Gibbs ensemble technique was found impracticable for temperatures $T^*<1.0$. As an (approximate) alternative, we performed a series of constant-pressure NPT Monte Carlo simulations of the liquid phase at $P^*=0$ for temperatures in the range $T^*\leqslant1.0$. Given that the coexistence pressure at $T^*=1.0$ is $P^*=0.000\,59(3)$, this procedure is expected to yield reliable estimates of the liquid densities at coexistence. Obviously, the estimates improve as T^* decreases. The corresponding results are included in Table II. It is important to note that even in the most unfavorable case ($T^*=1.0$), the resulting liquid density obtained with these NPT simulations [$\rho_\ell^*=0.4058(14)$] compares well with the value $\rho_\ell^*=0.4061(12)$ obtained using the Gibbs ensemble technique.

As well as determining the location of the triple point, it

TABLE II. Density ρ^* and residual internal energy (per particle) U^* in the liquid phase as obtained from NPT Monte Carlo simulations at zero pressure in a system of 500 2CLJ molecules with $L^*=1$.

T^*	ρ^*	U^*
1.00	0.4058(14)	−10.50(5)
0.95	0.4139(14)	−10.78(4)
0.90	0.4220(13)	−11.06(4)
0.85	0.4295(12)	−11.33(4)
0.80	0.4372(12)	−11.61(4)
0.75	0.4451(13)	−11.90(5)
0.70	0.4527(14)	−12.19(5)
0.68	0.4575(12)	−12.36(4)
0.66	0.4601(10)	−12.46(5)
0.64	0.4630(12)	−12.57(5)
0.62	0.4662(13)	−12.70(5)
0.6	0.4697(13)	−12.82(5)
0.58	0.4726(12)	−12.94(4)
0.56	0.4755(13)	−13.06(5)
0.54	0.4778(14)	−13.15(5)
0.52	0.4799(11)	−13.23(5)

TABLE III. Helmholtz free energies A for 2CLJ model systems with $L^*=1$ at two state points T^*, ρ^* for two solid structures. The simulation data were obtained from Einstein-crystal calculations (A_{EC}) for both the disordered solid and for the ordered solid labeled as CP1 (in Ref. 8). For the disordered solid, the entropic contribution due to the degeneracy of the fcc lattice (taken from Ref. 62) is added. Also included are the corresponding values obtained from Wertheim's TPT1 theory.

T^*	ρ^*	Method	Structure	$A_{EC}/(Nk_BT)$	Degeneracy	$A/(Nk_BT)$
1	0.5490	Simulation	Disordered solid	−4.17(3)	−1.5194	−5.69(3)
1	0.5490	Theory	Disordered solid			−5.69
1	0.5490	Simulation	Ordered CP1 solid	−4.76(3)	0	−4.76(3)
2	0.580	Simulation	Disordered solid	3.13(2)	−1.5194	1.61(2)
2	0.580	Theory	Disordered solid			1.65

is useful to consider the location of the critical point resulting from our Gibbs ensemble calculations. The critical temperature T_c and density ρ_c are obtained using the simulation results for the vapor and liquid coexistence densities and the relations

$$\rho_\ell^* - \rho_v^* = A(T^* - T_c^*)^\beta, \tag{5}$$

and

$$\frac{\rho_\ell^* + \rho_v^*}{2} = B + CT^*, \tag{6}$$

where ρ_ℓ^* and ρ_v^* are the liquid and vapor coexistence densities at temperature T^*, A, B, and C are constants, and β is the corresponding critical exponent; a value $\beta=1/3$ was assumed here. The critical pressure P_c^* is obtained using the relation

$$\ln P^* = a + bT^*, \tag{7}$$

where P^* is the saturation pressure at temperature T^*, and a and b are constants.

B. The solid phases

The simulation details regarding the solid phase are similar to those of previous works,[8,9,51] and hence we discuss here only the main features.

As mentioned in Sec. I we have considered two solid structures: An ordered CP1 structure[8] and a disordered structure. In the case of the CP1 solid structure, $N=256$ dimer molecules are arranged in four layers with 64 2CLJ molecules in each layer. Since the solid CP1 structure does not have cubic symmetry the Rahman–Parrinello[23] modification of the constant-pressure NPT Monte Carlo technique is used in order to allow for nonisotropic changes in the simulation box shape.[24] On the other hand, in the case of the disordered structure, an fcc close-packed arrangement of atoms with the molecular bonds randomly distributed[51] is generated. The number of molecules in the disordered solid was $N=432$. Two different random structures were generated and the results reported here correspond to the average obtained over those different configurations. Since the distribution of bonds in the solid phase is isotropic, an isotropic scaling of the volume is performed in these NPT simulations.

The simulations were started at very high pressures where the density is close to the close-packing limit (no true close-packing can be defined when a soft potential such as the LJ is used, but the reduced number density of the hard-sphere model at close packing can be used as a good starting point). After generating initial structures at the close-packing density, these were expanded to lower densities by performing NPT simulations at slowly decreasing pressures. A typical run of the solid phase involved 30 000 equilibration cycles followed by 30 000 cycles for obtaining equilibrium properties.

In order to determine the fluid–solid equilibrium, the free energy of the fluid and solid phases must be calculated. The residual free energy of the fluid phase A^{res} can be obtained by thermodynamic integration,

$$\frac{A^{res}(\rho,T)}{Nk_BT} = \int_0^\rho \frac{(Z(\rho,T')-1)}{\rho} d\rho - \int_{T'}^T \frac{U}{Nk_BT^2} dT. \tag{8}$$

Following Eq. (8), the free energies of the fluid phase at a temperature $T^*=2$ (supercritical temperature) were obtained via integration of the compressibility factor along the corresponding isotherm, while the free energies of the fluid phase at $T^*=1$ were obtained from those at $T^*=2$ integrating through isochores. In the case of the solid phase, the free energies can be calculated using the Einstein-crystal methodology.[25] The method used here is quite similar to the one described in previous works.[8,10,17] Translational and orientational springs are used, with a maximum value $\lambda_{max}=20\,000$ for both springs (note, however, that the units are of k_BT/σ^2 for the translational spring and of k_BT for the orientational spring). The free-energy calculations were performed at $T^*=1$ using ten different values of λ in the range $0\leqslant\lambda\leqslant\lambda_{max}$ and, as before, the length of the runs for the free-energy calculations was 30 000 equilibration cycles + 30 000 averaging cycles. In the case of the CP1 structure, it is important to mention that the shape of the equilibrium unit cell at a given density is slightly different from that of close packing; the free-energy calculations were carried out using the equilibrium unit cell at each density. The free energy for the disordered structures was evaluated by considering the average of two independent disordered configurations. The results of the free-energy calculations for both the CP1 structure and the disordered structures are given in Table III.

C. Gibbs–Duhem simulations

Once the free energies of the fluid and solid phases are known at a fixed temperature ($T^*=1$, in this work), the fluid–solid equilibrium can be determined by equating the pressures and chemical potentials of both phases. Results of

TABLE IV. Fluid–solid coexistence properties obtained using the Gibbs–Duhem integration scheme for the 2CLJ model system with $L^*=1$. The solid structure corresponds to that of the disordered solid. The initial equilibrium point for the Gibbs–Duhem integration was a state at $T^*=1$ and $P^*=4.37$. Two Gibbs–Duhem integration series were performed starting from the state at $T^*=1$, the first one was extended to higher temperatures and the second one to lower temperatures. The equilibrium state at $T^*=2$ with the asterisk was obtained from the Einstein-crystal calculations presented in Table III. ρ_f^* and ρ_s^* are the fluid and solid densities at fluid–solid coexistence, respectively.

T^*	P^*	ρ_f^*	ρ_s^*	T^*	P^*	ρ_f^*	ρ_s^*
2.1053	20.3695	0.5393	0.5835	1.0000	4.3700	0.4871	0.5354
2.0000	18.7356	0.5348	0.5798	0.9804	4.1131	0.4855	0.5342
2.0000*	18.5100	0.5347	0.5784	0.9615	3.8667	0.4839	0.5332
1.9048	17.2771	0.5311	0.5761	0.9434	3.6311	0.4827	0.5319
1.8182	15.9662	0.5278	0.5728	0.9259	3.4053	0.4816	0.5314
1.7391	14.7805	0.5242	0.5695	0.9091	3.1885	0.4803	0.5301
1.6667	13.7032	0.5214	0.5669	0.8929	2.9800	0.4794	0.5292
1.6000	12.7240	0.5182	0.5637	0.8772	2.7795	0.4786	0.5282
1.5385	11.8276	0.5154	0.5613	0.8621	2.5868	0.4773	0.5275
1.4815	11.0048	0.5125	0.5587	0.8475	2.4016	0.4768	0.5268
1.4286	10.2476	0.5104	0.5565	0.8333	2.2235	0.4759	0.5258
1.3793	9.5486	0.5075	0.5542	0.8197	2.0514	0.4746	0.5250
1.3333	8.9020	0.5054	0.5520	0.8065	1.8856	0.4734	0.5243
1.2903	8.2991	0.5030	0.5500	0.7937	1.7260	0.4730	0.5232
1.2500	7.7399	0.5012	0.5480	0.7812	1.5721	0.4720	0.5227
1.2121	7.2180	0.4990	0.5461	0.7692	1.4233	0.4712	0.5217
1.1765	6.7299	0.4970	0.5444	0.7576	1.2795	0.4705	0.5212
1.1429	6.2743	0.4948	0.5427	0.7463	1.1401	0.4690	0.5204
1.1111	5.8470	0.4936	0.5412	0.7353	1.0056	0.4684	0.5197
1.0811	5.4437	0.4915	0.5393	0.7246	0.8753	0.4675	0.5189
1.0526	5.0650	0.4897	0.5380	0.7143	0.7492	0.4665	0.5185
1.0256	4.7082	0.4882	0.5364	0.7042	0.6269	0.4655	0.5176
1.0000	4.3700	0.4871	0.5354	0.6944	0.5084	0.4656	0.5172
				0.6849	0.3930	0.4637	0.5166
				0.6757	0.2813	0.4631	0.5160
				0.6667	0.1727	0.4629	0.5152
				0.6579	0.0671	0.4621	0.5150
				0.6494	0.0003	0.4617	0.5147

the fluid–solid equilibrium at this temperature are reported in Table IV. In order to obtain the complete fluid–solid coexistence curve in a range of temperatures, the Gibbs–Duhem integration technique can be used. We have used a modified version of the Clausius equation

$$\left(\frac{dP}{dT}\right)=\frac{\Delta h}{T\Delta v}, \tag{9}$$

which can be written as

$$\left(\frac{\ln P}{d\beta}\right)=-\frac{\Delta h}{\beta P\Delta v}=f, \tag{10}$$

where $\beta=1/T$, and Δh and Δv are the enthalpy and volume changes per particle between the fluid and solid phases, respectively. The integration of Eq. (10) requires an initial coexistence point (here, the fluid–solid equilibrium results at $T^*=1$ are used), a simple trapezoidal rule can then be used with a step $\Delta\beta$. One assumes that for a certain temperature T_0, the coexistence pressure P_0 is known, and that we wish to calculate the coexistence pressure P_1 for a temperature T_1. An initial guess of P_1 is estimated as

$$P_{1,1}=P_0\exp(\Delta\beta f_0). \tag{11}$$

A simulation is then carried out at temperature T_1 and pressure $P_{1,1}$, and the right-hand side of Eq. (10) (i.e., the function $f_{1,1}$) is evaluated. A second guess for P_1 is given by

$$P_{1,2}=P_0\exp(\Delta\beta(f_0+f_{1,1})/2). \tag{12}$$

A simulation at temperature T_1 and pressure $P_{1,2}$ is carried out, and the right-hand side of Eq. (10) (i.e., the function $f_{1,2}$) evaluated. Similarly, a third guess for P_1 is

$$P_{1,3}=P_0\exp(\Delta\beta(f_0+f_{1,2})/2). \tag{13}$$

Finally, the estimate of the coexistence pressure P_1 corresponding to T_1 is obtained as

$$P_1=(P_{1,2}+P_{1,3})/2. \tag{14}$$

The length of the runs at each $P_{1,1}$, $P_{1,2}$, and $P_{1,3}$ were typically of 5000 equilibration cycles and 5000 averaging cycles. Once the coexistence pressure for a temperature is determined, runs of $30\,000+30\,000$ cycles are used to determine the equilibrium properties at coexistence. We have typically used a step $\Delta 3^*=\Delta 3\epsilon=0.02$ in the integration. The algorithm was checked by implementing this Gibbs–Duhem integration scheme to determine the fluid–solid equilibrium properties of a LJ monomer system; excellent agreement with previous results obtained by other authors was found.[59,61] We estimate the uncertainty of our Gibbs–Duhem simulation results to be approximately 0.5%.

In the implementation of the Gibbs–Duhem method, we have carried out isotropic NPT simulations for the fluid phase, isotropic NPT simulations for the disordered solid structure, and nonisotropic NPT simulations for the ordered solid structure. The Gibbs–Duhem calculations were run on a dual Athlon XP2000 and a parallel version of the program was developed using OPENMP. In this way, the Gibbs–Duhem simulations were almost twice as fast as those undertaken on a single processor.

IV. RESULTS

First, we examine the vapor–liquid equilibria. In Table I, the results of the vapor–liquid Gibbs ensemble simulations can be seen and, in Table II, the NPT simulations at zero pressure are presented. The estimated critical properties of the 2CLJ fluid obtained using the computer simulation data in this work are $T_c^*=1.784(7)$, $\rho_c^*=0.144(3)$, and $P_c^*=0.103(13)$. These results are in good agreement with the previous estimates of Dubey *et al.*[26] ($T_c^*=1.78(1)$, and $\rho_c^*=0.149(1)$). In Figs. 1 and 2, the vapor–liquid coexistence densities and the vapor pressure curve obtained from our simulations and from Wertheim's TPT1 are presented, respectively. The results of Dubey *et al.*[26] are also included for comparison. As expected, Wertheim's TPT1 provides a very good description of the vapor–liquid coexistence properties (densities and pressures) of the 2CLJ model fluid.

Let us now focus on the properties of the solid phase. In Sec. II, we provided the main expressions of the EOS of the 2CLJ model in the solid phase following the TPT1 framework of Wertheim; the equation was presented in a previous work,[51] and additional details can be found therein. The free energies of the solid phases obtained by computer simulation in this work are presented in Table III. As mentioned earlier,

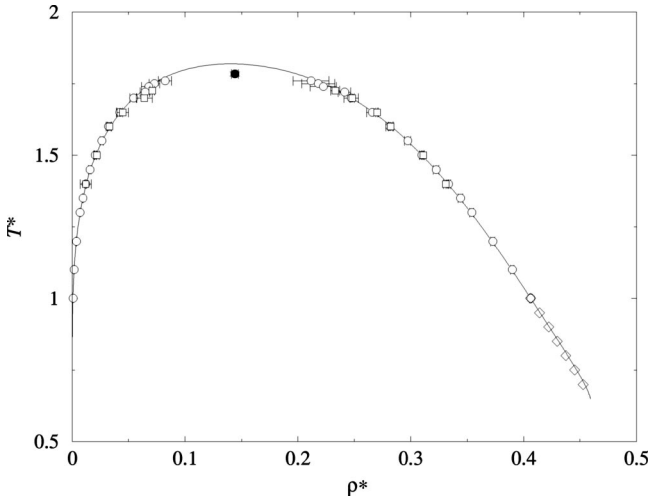

FIG. 1. Vapor–liquid coexistence curve ($T-\rho$ representation) for the 2CLJ model system with $L^*=1$ from computer simulation (symbols) and predictions from Wertheim's TPT1 (curve). The open circles correspond to the Gibbs ensemble Monte Carlo simulation results obtained in this work, the squares to the Gibbs ensemble data obtained by other authors (see Ref. 26), the diamonds to the liquid densities obtained in this work using NPT Monte Carlo simulations at zero pressure, and the closed circle to the critical point [estimated by the scaling relations given by Eqs. (5) and (6)].

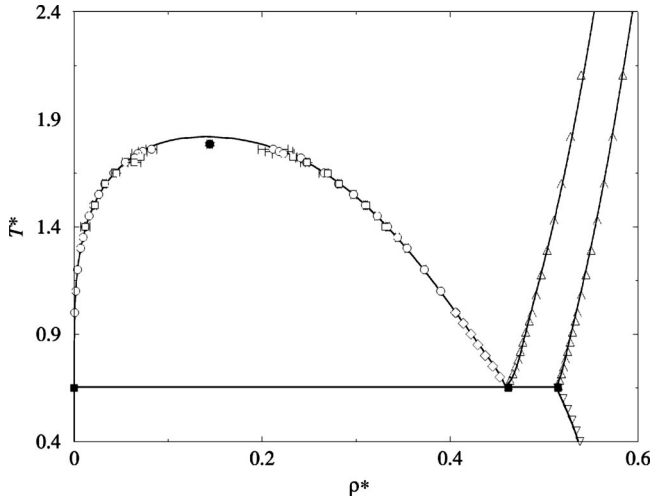

FIG. 3. $T-\rho$ representation of the global phase diagram (including vapor, liquid, and solid phases) for the 2CLJ model system with $L^*=1$ from simulation results (symbols) and predictions from Wertheim's TPT1 (solid curves). The closed squares correspond to the triple-point properties estimated from simulation, the ''up'' triangles to the fluid–solid coexistence data obtained from Gibbs–Duhem simulations, and the inverted triangles to the vapor–solid coexistence data obtained from NPT simulations at zero pressure. The remaining symbols are the same as those in previous figures.

in the case of the disordered solid structure, the results correspond to the average of two independent disordered configurations. In Table III, the calculated free energies using Wertheim's TPT1 have also been included. It can be seen that the theoretical approach provides accurate predictions of the free energy of the disordered solid. It is important to note here that, in order to obtain the free energy of the disordered solid, the contribution of the degeneracy entropy must be added to the free energy obtained from the Einstein-crystal calculations. This is due to the fact that this method provides the free energy associated with a given solid configuration and, therefore, the degeneracy entropy must be added to account for the number of ways of organizing a disordered solid configuration. In the case of dimer molecules on an fcc lattice, the estimation of the number of ways of arranging the configuration is known as the ''dimer problem.'' Nagle[62] proposed an accurate estimate of the degeneracy entropy giving $A/(Nk_BT)=-1.5194$. It is clear from Table III that, for a given density, the free energy of the disordered solid is lower than that of the ordered CP1 solid, meaning that the stable solid structure for the 2CLJ model corresponds to the disordered solid and not to the ordered CP1 solid. This was first shown in a two-dimensional hard-disk dimer system by Wojciechowski *et al.*;[52,53] our results indicate that the same conclusion holds true in the case of a three-dimensional 2CLJ solid. It is important to note, however, that (stable) disordered structures are not possible for values of L^* significantly different from unity. For values of L^* less than 1, the stable solid phase is expected to exhibit an ordered structure; i.e., the singular nature of the model with $L^*=1$ makes the existence of the disordered solid possible.

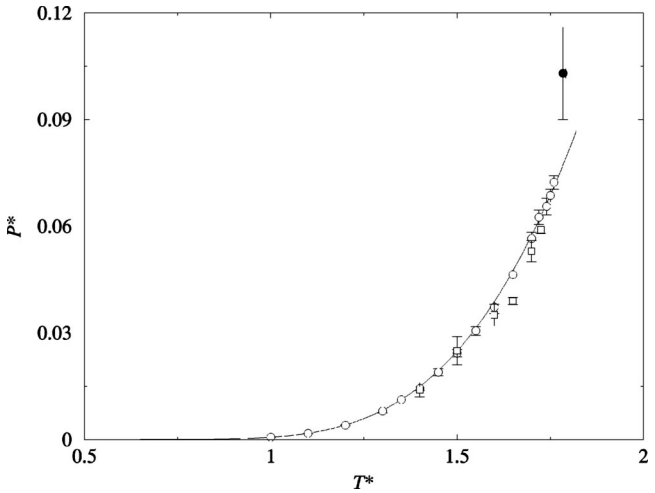

FIG. 2. Vapor pressure curve ($P-T$ representation) for the 2CLJ model system with $L^*=1$ from computer simulation (symbols) and predictions from Wertheim's TPT1 (curve). See Fig. 1 for details of the symbols.

Once the free energy of the solid is known, it is possible to determine the fluid–solid equilibrium for a given temperature. The equilibrium pressure corresponding to a temperature $T^*=1$ is found to be $P^*=4.37$. This coexistence point can then be used as the starting point for the Gibbs–Duhem integration. Representative coexistence points obtained using the Gibbs–Duhem integration method are presented in Table IV. In Fig. 3, the temperature–density projection of the global (solid–liquid–vapor) phase diagram for a 2CLJ model system is shown, and in Fig. 4, the pressure–temperature projection is presented. The triple-point temperature, estimated using the simulation results of this work, is found to be $T_t^*=0.650(4)$. This temperature is found both by extrapolating the fluid–solid coexistence pressure to zero (the pressure at the triple point is expected to be very close to zero), and by finding the temperature at which the density of the fluid at zero pressure becomes identical to that of the fluid at the fluid–solid coexistence curve. The corresponding

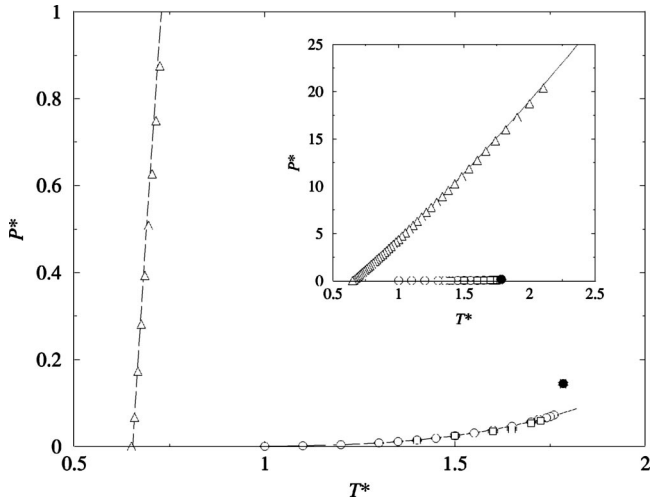

FIG. 4. $P-T$ representation of the global phase diagram (vapor, liquid, and solid phases) for the 2CLJ model system with $L^*=1$ from simulation results (symbols) and Wertheim's TPT1 (solid curves). See Fig. 3 for details of the symbols. The inset shows the $P-T$ diagram at high pressure.

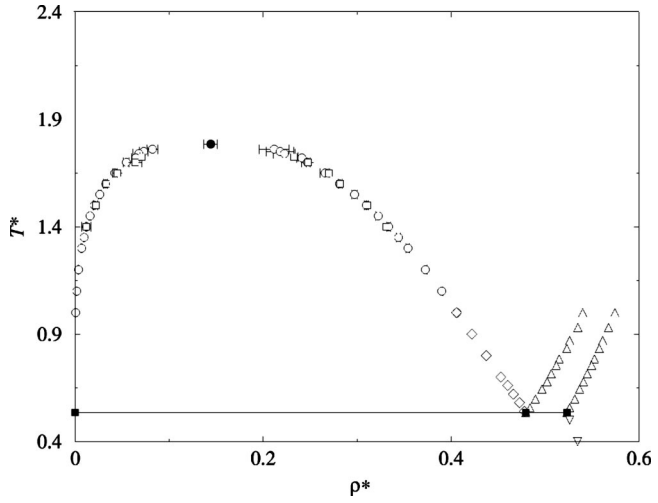

FIG. 6. $T-\rho$ representation of the global phase diagram of the 2CLJ system obtained in this work from Gibbs–Duhem simulations in the case of an ordered CP1 solid phase. The symbols have the same meaning as those in Fig. 3.

coexistence densities at the triple point are $\rho_f^*=0.462$, and $\rho_s^*=0.515$. In Figs. 3 and 4, the results obtained using the equations based on Wertheim's TPT1 are also included. It is clearly seen that the theory provides an accurate description of the coexistence properties of the 2CLJ model, including the fluid–solid equilibria. The theory predicts a triple point at $T_t^*=0.653$, in excellent agreement with the simulation result. The triple-point temperature in a LJ monomer system predicted by the theory (i.e., $m=1$ here) is found to be $T_t^*=0.687$, which is also in excellent agreement with the computer simulation estimate of Agrawal and Kofke[61] ($T_t^*=0.687$). As can be seen, the triple-point temperature of the LJ dimer is 5% lower than that of the LJ monomer. The comparison can be seen more clearly in Fig. 5, where the phase diagram of the monomer LJ and of the 2CLJ model systems are shown. Note that in the Fig. 5, the density is expressed as the number of monomers per unit volume.

It is also useful to compare these results with those of the case in which the ordered structure of 2CLJ molecules is considered to be the stable phase. In Fig. 6, the phase diagram in such a case is presented. Results for the fluid-ordered solid transition found from Gibbs–Duhem simulations are presented in Table V. The triple point in this case would be located at $T_t=0.534(5)$. The lower stability of the ordered phase provokes a decrease in the triple-point temperature, shifting the fluid–solid equilibrium to higher densities. The triple-point temperature of the 2CLJ model system with $L^*=0.67$ has been determined by Lisal and

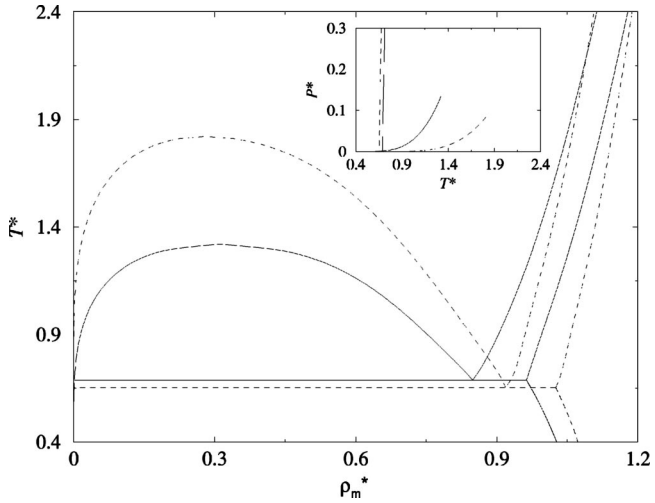

FIG. 5. $T-\rho$ representation of the global phase diagram (vapor, liquid, and solid phases) of the LJ system (solid curves), and that of the 2CLJ model system with $L^*=1$ (dashed curves). The reduced number density of monomers is denoted as $\rho_m^*=m\rho^*$.

TABLE V. Fluid–solid coexistence conditions obtained using the Gibbs–Duhem integration method for a 2CLJ model system with $L^*=1$. The solid structure corresponds to that of the ordered CP1 solid. The initial equilibrium point for the Gibbs–Duhem integration was a state at $T^*=1$ and $P^*=11.10$. The density at coexistence of the fluid is denoted as ρ_f^*, whereas that of the solid is denoted as ρ_s^*.

T^*	P^*	ρ_f^*	ρ_s^*
1.0000	11.1000	0.5399	0.5741
0.9524	9.8125	0.5346	0.5693
0.9091	8.6666	0.5318	0.5653
0.8696	7.6431	0.5259	0.5612
0.8511	7.1734	0.5233	0.5595
0.8163	6.3058	0.5191	0.5560
0.7843	5.5254	0.5149	0.5524
0.7692	5.1614	0.5141	0.5510
0.7407	4.4873	0.5107	0.5476
0.7143	3.8734	0.5064	0.5448
0.6897	3.3110	0.5031	0.5419
0.6780	3.0481	0.5014	0.5409
0.6431	2.2769	0.4966	0.5365
0.6116	1.5988	0.4921	0.5331
0.5831	0.9989	0.4882	0.5293
0.5571	0.4648	0.4825	0.5260
0.5494	0.3077	0.4830	0.5253
0.5347	0.0209	0.4794	0.5232

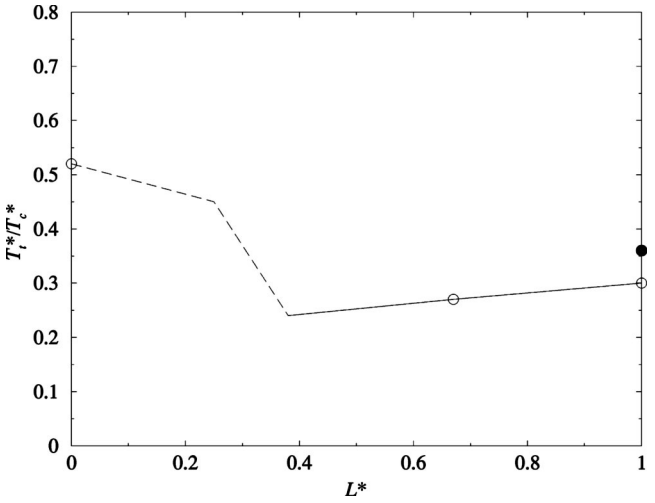

FIG. 7. Sketch of the T_t/T_c ratio for 2CLJ model systems. (See Refs. 61 and 36, respectively, for the results for $L^*=0$ and those corresponding to $L^*=0.67$.) The results for $L^*=1$ were obtained in this work, both for the ordered (open circle) and disordered solid structures (filled circle). The solid line connects the simulation results (of Ref. 36) with those of the ordered solid of this work. The dashed line is a sketch, and is not based on calculations.

Vacek[36] at $T_t^*=0.62$ (in this case, the stable structure of the solid is the ordered one). When compared to the critical point, the ratio T_t/T_c in the system with $L^*=0.67$ takes a value $T_t/T_c=0.27$, while for the model with $L^*=1$ this ratio takes a value $T_t/T_c=0.36$ when the (stable) disordered structure is considered, and $T_t/T_c=0.30$ when the ordered CP1 structure is assumed. These calculations show that for the ordered solid, the ratio T_t/T_c is roughly constant with a value of about 0.27, and slowly increases with L^*. This conclusion holds for systems with bond lengths $L^*>0.4$ (no plastic crystal phases are possible).[63] A marked difference is noted in comparison with the T_t/T_c ratio of the LJ monomer fluid ($T_t/T_c=0.687/1.31=0.52$). In summary, the triple-point temperature is about 0.3 of the critical point in the case of 2CLJ fluids with $L^*>0.4$, but it is 1/2 of the critical temperature in monomer LJ fluids. More work is needed to assess the variation of T_t/T_c with L^*, especially in the range of small values of L^* where plastic crystal phases are possible. However, the results of this work allow one to obtain a tentative value for the ratio T_t/T_c of 2CLJ models of varying L^*. This is presented in Fig. 7. The results of this work are in line with the predictions of the mean-field theory proposed by Paras *et al.*[63]

Let us finish by discussing the phase behavior of the 2CLJ at very low temperatures. For the range of temperatures considered so far (above the triple point), the disordered solid phase was found to be the stable phase. However, it is not clear which is the stable solid phase at very low temperatures, since the ordered and disordered solids have different thermodynamic properties. The differences may be summarized as follows. For a certain temperature and density, the ordered solid has a slightly higher pressure, and a slightly lower internal energy, than the disordered solid. Zero-pressure densities of the ordered solid are slightly smaller than those of the disordered solid. The differences are small, but clearly visible. Simulations results for ordered and disordered solids were presented in tabular form in Ref. 51 and shall not be reproduced here. In order to evaluate the free energy of the ordered and disordered solid phases at low temperatures, we have performed NVT simulations of the solid phase at constant density $\rho^*=0.549$ (using the equilibrium shape of the unit cell), starting at temperature $T^*=1$ and ending at $T^*=0.20$. Thermodynamic integration yields the following expression for the free energies of the solid phase along the isochore:

$$\frac{A}{Nk_BT}(\rho^*=0.549,T^*)=\frac{A}{Nk_BT}(\rho^*=0.549,T^*=1)-\int_1^{T^*}\frac{U}{N\epsilon(T^*)^2}dT^*. \qquad (15)$$

To perform the integral of Eq. (15), we have fitted the residual internal energy to the following expression:

$$\frac{U}{N\epsilon}=c_0+c_1T^*+c_2(T^*)^2+c_3(T^*)^3+c_4(T^*)^4. \qquad (16)$$

The values of coefficients c_0-c_4 from Eq. (16), corresponding to the ordered solid, are -16.538, 2.3769, $-0.074\,064$, $-0.141\,85$, and $0.090\,332$, whereas those for the disordered solid are -16.223, 2.5488, $-0.38\,096$, $0.271\,78$, and $-0.116\,38$. The values of the free energy at the reference state defined by $\rho^*=0.549$ and $T^*=1$ for the ordered and disordered solids were taken from Table III. It was found that the Helmholtz free energies of the ordered and disordered solids were identical for $\rho^*=0.549$ and $T^*=0.28$. NPT simulations were performed for both the ordered and disordered solids at $T^*=0.28$, and the EOS and chemical potentials were evaluated for both types of solids. It was found that at low pressures, the ordered solid was more stable (lower chemical potential for a certain pressure) than the disordered solid. At high pressures, the disordered solid turns out to be the stable phase. We locate the first-order phase transition between the ordered and the disordered solid phase at $P^*=0.54$ for $T^*=0.28$. Taking this state as the initial equilibrium point, Gibbs–Duhem integration was performed in order to evaluate the coexistence line between the ordered and the disordered solid. Results are presented in Table VI and Figs. 8 and 9. As can be seen, the ordered solid is indeed the stable phase at low temperatures and pressures. The vapor-ordered solid-disordered solid triple point is located at $T^*=0.282$, the densities of the ordered and disordered solids being $\rho_o^*=0.5433$ and $\rho_d^*=0.5462$, respectively. It is noticeable in Fig. 8 that the density jump between the two solid phases is small, and in Fig.9 that the slope of the ordered solid–disordered solid phase transition is negative. Using the Clapeyron relation, it can be shown that the negative slope follows from a negative value of Δv (the disordered solid has a higher density than the ordered one) and a positive value of Δh (the disordered solid has a higher enthalpy than the ordered solid). Is it possible to provide a simple explanation for the fact that the ordered solid is the stable phase at low temperatures? Notice that we are using classical statistical thermodynamics here (although for a real substance at such low temperatures, a quantum

TABLE VI. Ordered solid–disordered solid coexistence conditions obtained using the Gibbs–Duhem integration method for a 2CLJ model system with $L^*=1$. The initial equilibrium point for the Gibbs–Duhem integration was a state at $T^*=0.28$ and $P^*=0.54$. The density at coexistence of the ordered solid is denoted as ρ_o^*, whereas that of the disordered solid is denoted as ρ_d^*.

T^*	P^*	ρ_o^*	ρ_d^*
0.2800	0.5400	0.5476	0.5507
0.2652	2.8245	0.5627	0.5657
0.2518	4.7287	0.5729	0.5761
0.2397	6.4268	0.5812	0.5846
0.2288	7.8639	0.5876	0.5914
0.2141	9.6654	0.5953	0.5995
0.2011	11.1460	0.6013	0.6057
0.1897	12.4245	0.6063	0.6109
0.1795	13.5732	0.6107	0.6152
0.1522	16.8007	0.6221	0.6266
0.1321	19.3293	0.6302	0.6346
0.1167	21.3610	0.6365	0.6408
0.1045	23.0255	0.6414	0.6457

treatment would be required). The key issue is that for a certain density, the internal energy of the ordered solid is lower than that of the disordered solid. This is due to the fact that the ordered solid is noncubic and can distort (relax) the lattice parameters in an attempt to decrease the internal energy. The disordered solid cannot optimize the parameters of the unit cell since the distribution of bonds in the solid is isotropic. Notice that we are using anisotropic NPT Monte Carlo (Rahman–Parrinello type) for the ordered solid and isotropic NPT for the disordered solid. In the integrand of Eq. (15), the internal energy appears as divided by $(1/T^2)$.

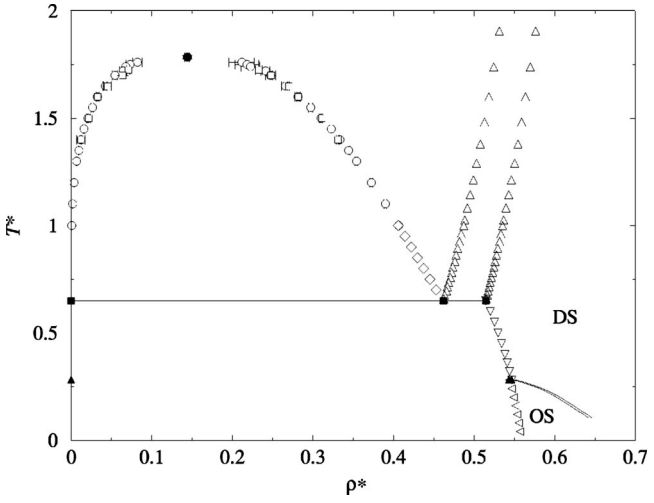

FIG. 8. Global phase diagram (in the $T-\rho$ representation) of the 2CLJ model as obtained from the simulation results of this work. The solid lines correspond to the ordered–disordered solid coexistence curve, the up filled triangles to the vapor-ordered solid-disordered solid triple-point obtained from Gibbs–Duhem integration, the "left-hand side" triangles to the vapor-ordered solid coexistence data obtained from NPT simulations at zero pressure, and the remaining symbols are the same as those in Fig. 3. The regions of stability of the ordered solids (OS) and disordered solids (DS) solids are also shown. Two triple points appear in the phase diagram: The vapor–liquid-disordered solid point, located at $T_t^*=0.650$ (filled squares), and the vapor-ordered solid-disordered solid point, located at $T_t^*=0.282$ (filled triangles).

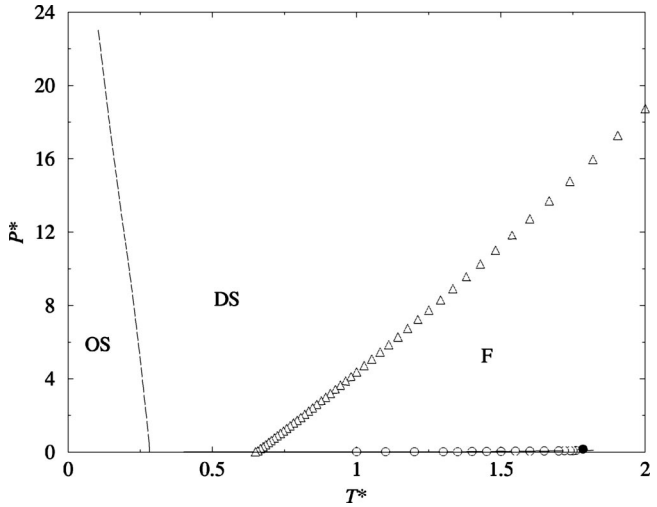

FIG. 9. Global phase diagram (in the $P-T$ representation) of the 2CLJ model as obtained from the simulation results of this work. The solid line corresponds to the disordered solid–ordered solid coexistence obtained from Gibbs–Duhem integration, and the symbols are the same as those in Fig. 4. The regions of stability of the fluid (F), the OS and the DS are also shown. Two triple points appear in the phase diagram: The vapor–liquid-disordered solid and vapor-ordered solid-disordered solid points. The pressure curves associated with both sublimation lines (vapor-ordered solid and vapor-disordered solid) are not visible on the scale.

Therefore, the integrand becomes large at low temperatures and differences between ordered and disordered solids can be significant at low temperatures. In fact, this is exactly what happens. The lower internal energy of the ordered solid is able to compensate for the absence of the degeneracy entropy. This leads to the appearance of an small region of stability for the ordered solid in the phase diagram.

V. CONCLUSIONS

The global phase diagram of 2CLJ model molecules with $L^*=1$ has been determined by computer simulation. The vapor–liquid equilibria was obtained using Gibbs ensemble simulations and NPT simulations at zero pressure were used to determine the orthobaric densities at low temperatures. In terms of the fluid–solid equilibria, free-energy calculations at a given temperature and density were first carried out, and the equilibrium at the specified point was obtained. The Gibbs–Duhem integration method was then used to determine the complete fluid–solid coexistence curve. It is found that the equilibrium solid structure for the 2CLJ with $L^*=1$ corresponds to a disordered solid in which the atoms form an fcc lattice but the molecular bonds are oriented randomly within the lattice. The corresponding triple-point properties are found to be $T_t^*=0.650$, $\rho_f^*=0.462$, and $\rho_s^*=0.515$. As was found for two-dimensional disk dimers and for fully flexible hard-sphere chains, the stable solid structure is a disordered one. This seems to be a general feature of fully flexible models of chain molecules formed by tangent monomers. Wojciechowski *et al.*[52,53] suggested this possibility. Note, however, that the equilibrium solid structures in models with arbitrary values of L^* are not expected to be disordered; it is likely that molecular systems with a bond length L^* different from 1 will exhibit ordered

structures as the stable solid phases. We have shown that Wertheim's TPT1 can be used to study both fluid and solid phases of chainlike LJ molecules. The theoretical approach provides not only an accurate EOS, but also accurate values of the free energies for both fluid and solid phases. As a result, we have been able to show the excellent agreement found between the computer simulation phase equilibrium data and the calculated phase diagram for the 2CLJ model system, including the vapor–liquid–solid triple point. This article validates the fact that Wertheim's TPT1 can be used to predict phase diagrams of fully flexible LJ chains as was first shown in Ref. 51. By comparing the triple-point temperature T_t of the 2CLJ with that of the monomer, it is found that the dimer system has a T_t 5% lower than that of the monomer system.

The fluid–solid equilibrium between the fluid and an ordered solid has also been obtained by means of computer simulations. In this case, the triple point is found at $T_t^* = 0.534$, which means that the ratio $T_t/T_c = 0.30$ for the ordered solid with $L^* = 1$. Lisal and Vacek[36] evaluated this ratio for a system with $L^* = 0.67$ obtaining $T_t/T_c = 0.27$. It seems that in 2CLJ systems, the ratio T_t/T_c slowly increases with L^* in the region where the stable solid phase is ordered, i.e., $0.4 \leqslant L^* < 1$, as was predicted some time ago using a mean-field approach.[63]

For the model considered here, the 2CLJ with $L^* = 1$, the disordered solid was found to be the stable solid phase for most of thermodynamic conditions. However, it has been found that at very low temperatures (substantially below the triple point), the stable solid phase is an ordered solid. The lower internal energy of the ordered solid is able to compensate for the absence of the degeneracy entropy leading to the appearance of an small region of stability for the ordered solid.

ACKNOWLEDGMENTS

Financial support is due to project Nos. BFM-2001-1420-C02-01 and BFM-2001-1420-C02-02 of Spanish DGICYT (Dirección General de Investigación Científica y Técnica). One of the authors (A.G.) would also like to thank the Engineering and Physical Sciences Research Council for the award of an Advanced Research Fellowship. E.d.M. and F.J.B. also acknowledge the Junta de Andalucia and Universidad de Huelva for additional financial support.

[1] W. G. Hoover and F. H. Ree, J. Chem. Phys. **49**, 3609 (1968).
[2] B. J. Alder, W. G. Hoover, and D. A. Young, J. Chem. Phys. **49**, 3688 (1968).
[3] J. P. Hansen and L. Verlet, Phys. Rev. **184**, 151 (1969).
[4] D. Frenkel and B. M. Mulder, Mol. Phys. **55**, 1171 (1985).
[5] P. Bolhuis and D. Frenkel, J. Chem. Phys. **106**, 666 (1997).
[6] J. A. C. Veerman and D. Frenkel, Phys. Rev. A **45**, 5632 (1992).
[7] S. J. Singer and R. J. Mumaugh, J. Chem. Phys. **93**, 1278 (1990).
[8] C. Vega, E. P. A. Paras, and P. A. Monson, J. Chem. Phys. **96**, 9060 (1992).
[9] C. Vega, E. P. A. Paras, and P. A. Monson, J. Chem. Phys. **97**, 8543 (1992).
[10] C. Vega and P. A. Monson, J. Chem. Phys. **102**, 1361 (1995).
[11] A. P. Malanoski and P. A. Monson, J. Chem. Phys. **107**, 6899 (1997).
[12] P. A. Monson and D. A. Kofke, Adv. Chem. Phys. **115**, 113 (2000).
[13] C. Vega, F. Bresme, and J. L. F. Abascal, Phys. Rev. E **54**, 2746 (1996).
[14] F. Bresme, C. Vega, and J. L. F. Abascal, Phys. Rev. Lett. **85**, 3217 (2000).
[15] B. Smit, K. Esselink, and D. Frenkel, Mol. Phys. **87**, 159 (1996).
[16] E. de Miguel, L. F. Rull, M. K. Chalam, and K. E. Gubbins, Mol. Phys. **74**, 405 (1991).
[17] E. de Miguel and C. Vega, J. Chem. Phys. **117**, 6313 (2002).
[18] L. A. Baez and P. Clancy, J. Chem. Phys. **103**, 9744 (1995).
[19] A. Z. Panagiotopoulos, Mol. Phys. **61**, 813 (1987).
[20] A. Lotfi, J. Vrabec, and J. Fischer, Mol. Phys. **76**, 1319 (1992).
[21] D. A. Kofke, Mol. Phys. **78**, 1331 (1993).
[22] D. A. Kofke, J. Chem. Phys. **98**, 4149 (1993).
[23] M. Parrinello and A. Rahman, Phys. Rev. Lett. **45**, 1196 (1980).
[24] S. Yashonath and C. N. R. Rao, Mol. Phys. **54**, 245 (1985).
[25] D. Frenkel and A. J. C. Ladd, J. Chem. Phys. **81**, 3188 (1984).
[26] G. S. Dubey, S. O'Shea, and P. A. Monson, Mol. Phys. **80**, 997 (1993).
[27] G. Galasi and D. J. Tildesley, Mol. Simul. **13**, 11 (1994).
[28] J. Stoll, J. Vrabec, H. Hasse, and J. Fischer, Fluid Phase Equilibria **179**, 339 (2001).
[29] M. Lisal, R. Budinsky, and V. Vacek, Fluid Phase Equilibria **135**, 193 (1997).
[30] C. Kriebel, A. Muller, J. Winkelmann, and J. Fischer, Mol. Phys. **84**, 381 (1995).
[31] M. Lombardero, J. L. F. Abascal, and S. Lago, Mol. Phys. **42**, 999 (1981).
[32] J. Fischer, J. Chem. Phys. **72**, 5371 (1980).
[33] D. B. McGuigan, M. Lupkowski, D. M. Paquet, and P. A. Monson, Mol. Phys. **67**, 33 (1989).
[34] J. Fischer, R. Lustig, M. Breitenfelder-Manske, and W. Lemming, Mol. Phys. **52**, 485 (1984).
[35] C. T. Lin and G. Stell, J. Chem. Phys. **114**, 6969 (2001).
[36] M. Lisal and V. Vacek, Mol. Simul. **19**, 43 (1997).
[37] M. S. Wertheim, J. Stat. Phys. **35**, 19 (1984).
[38] M. S. Wertheim, J. Stat. Phys. **35**, 35 (1984).
[39] M. S. Wertheim, J. Stat. Phys. **42**, 459 (1986).
[40] M. S. Wertheim, J. Stat. Phys. **42**, 477 (1986).
[41] M. S. Wertheim, J. Chem. Phys. **87**, 7323 (1987).
[42] W. G. Chapman, G. Jackson, and K. E. Gubbins, Mol. Phys. **65**, 1057 (1988).
[43] W. G. Chapman, J. Chem. Phys. **93**, 4299 (1990).
[44] J. K. Johnson, J. A. Zollweg, and K. E. Gubbins, Mol. Phys. **78**, 591 (1993).
[45] J. K. Johnson, E. A. Muller, and K. E. Gubbins, J. Phys. Chem. **98**, 6413 (1994).
[46] F. J. Blas and L. F. Vega, Mol. Phys. **92**, 1 (1997).
[47] F. J. Blas and L. F. Vega, J. Chem. Phys. **115**, 4355 (2001).
[48] C. Vega and L. G. MacDowell, J. Chem. Phys. **114**, 10411 (2001).
[49] F. J. Blas, A. Galindo, and C. Vega, Mol. Phys. **101**, 449 (2003).
[50] C. McBride and C. Vega, J. Chem. Phys. **116**, 1757 (2002).
[51] C. Vega, F. J. Blas, and A. Galindo, J. Chem. Phys. **116**, 7645 (2002).
[52] K. W. Wojciechowski, A. C. Branka, and D. Frenkel, Physica A **196**, 519 (1993).
[53] K. W. Wojciechowski, D. Frenkel, and A. C. Branka, Phys. Rev. Lett. **66**, 3168 (1991).
[54] E. A. Muller and K. E. Gubbins, Ind. Eng. Chem. Res. **40**, 2193 (2001).
[55] J. P. Hansen and I. R. McDonald, *Theory of Simple Liquids* (Academic, New York, 1986).
[56] D. A. McQuarrie, *Statistical Mechanics* (Harper and Row, New York, 1976).
[57] R. P. Sear and G. Jackson, J. Chem. Phys. **102**, 939 (1995).
[58] N. Elvassore and J. M. Prausnitz, Fluid Phase Equilibria **194**, 567 (2002).
[59] M. A. van der Hoef, J. Chem. Phys. **113**, 8142 (2000).
[60] M. P. Allen and D. J. Tildesley, *Computer Simulation of Liquids*, 2nd ed. (Clarendon, Oxford, 1987).
[61] R. Agrawal and D. A. Kofke, Mol. Phys. **85**, 43 (1995).
[62] J. F. Nagle, Phys. Rev. **152**, 190 (1966).
[63] E. P. A. Paras, C. Vega, and P. A. Monson, Mol. Phys. **79**, 1063 (1993).